# Liquid-gas phase transitions in a multicomponent nuclear system with Coulomb and surface effects

S. J. Lee* and A. Z. Mekjian
*Department of Physics and Astronomy, Rutgers University, Piscataway, New Jersey 08855*
(Received 26 June 2000; published 16 March 2001)

The liquid-gas phase transition is studied in a multicomponent nuclear system using a local Skyrme interaction with Coulomb and surface effects. Some features are qualitatively the same as the results of Müller and Serot where a relativistic mean field was used without Coulomb and surface effects. Surface tension brings the coexistence binodal surface to lower pressure. The Coulomb interaction makes the binodal surface smaller and causes another pair of binodal points at low pressure and large proton fraction with fewer protons in the liquid phase and more protons in the gas phase.

DOI: 10.1103/PhysRevC.63.044605 PACS number(s): 24.10.Pa, 21.65.+f, 05.70.−a, 64.10.+h

## I. INTRODUCTION

The liquid-gas phase transition in nuclei was first studied using a Skyrme interaction and focused mostly on one-component systems of just nucleons even though expressions were developed for two-component systems of protons and neutrons [1]. The phase transition aspects are considerably easier to study in one-component systems rather than two, where, for example, one has to deal with separate proton and neutron chemical potentials for charge and nucleon number conservation. Initial fragmentation models also mostly dealt with one-component systems. Such fragmentation studies gave the first evidence for the liquid-gas phase transition in nuclear systems [2,3]. Since then, the liquid-gas phase transition has been extensively studied experimentally and theoretically. Several reviews exist on this topic [4–6].

Because of the two-component nature of real nuclear systems, an analysis of liquid-gas phase transitions in these systems is important. Some preliminary results were reported in Ref. [1], and a very detailed study was done by Müller and Serot [7] who used a relativistic mean field model to develop the main thermodynamic properties of asymmetric nuclear matter. One interesting new aspect of two-component systems compared to one-component systems is that the phase transition is a second-order transition in their approach. The importance of the number of components on the order of the transition was pointed out by Glendenning [8]. Another interesting aspect of two-component systems is the possibility of having different proton-neutron ratios in the liquid and gas phases because of the symmetry energy, while still conserving the overall initial proton fraction. The study of nuclear systems with arbitrary proton-neutron ratios is important for radioactive beam experiments and in astrophysical situations such as in neutron stars. Because of the extra degree of freedom associated with varying proton fraction $y$ in the two phases, the phase diagram has a higher dimensionality and now becomes a surface in pressure $P$, temperature $T$, and proton fraction $y$ or nucleon density $\rho$. For one-component systems the phase diagram is represented as a binodal curve of $P$ versus density $\rho$ or volume $V$, whose end points at fixed $T$ give the liquid and gas densities. The Maxwell pressure versus $T$ in one-component systems is a line that terminate at the critical temperature $T_c$. For two-component systems, the binodal surface associated with phase coexistence in $(P,T,y)$ now contains some new elements [7]. One new element is a line of critical points (LCP) having the same densities both in liquid and gas phases. A second new element is a line of maximal asymmetry (LMA) in the neutron-proton ratio. A third new line arises as a line of equal concentration (LEC) having the same proton concentration $y$ in both liquid and gas phases with different nucleon density $\rho$. These lines come from the intersection of the binodal surface with fixed $T$ planes. For a fixed $T$ this intersection forms a loop of $P$ versus $y$. The condition $(dy/dP)_T=0$ gives the point of maximal asymmetry (MA) or smallest proton ratio at that $T$ and the condition $(dP/dy)_T=0$ with $(d^2P/dy^2)_T<0$ gives a critical point (CP) at that $T$. On the other hand, both the liquid side and gas side of the binodal curve come together with equal concentration (EC) of $y$ at the minimum pressure of the binodal curve at that $T$. The LMA, LCP, and LEC are then generated by considering these points as a function of $T$. Without a Coulomb interaction, the symmetry energy brings the LEC to $y=0.5$. For the interaction used in Ref. [7], the LEC is the same as the intersection of the binodal surface with the plane $y=0.5$ of a symmetric system and is the same as for a one-component system. The extreme end points of these lines are the same point, which is the critical point at $T_c$.

In this paper we extend the initial study of Ref. [1] using a Skyrme interaction in a similar way as done in Ref. [7]. Some features are qualitatively the same as in Ref. [7], but quantitatively differ because of the different interaction. Our equation of state based on the Skyrme interaction with Coulomb and surface effects has some features also not present in Ref. [7] which will also be discussed. According to the results of Ref. [7] which has no Coulomb interaction, the liquid phase has a higher proton fraction than the gas phase of mixed phases in the coexistent state. A real nucleus has fewer protons than neutrons due to the Coulomb interaction. For a given $A=N+Z$ stability is determined by Coulomb and symmetry energy effects. Since a stable finite nucleus has zero internal pressure while the gas phase has positive pressure [9], we also need to consider surface effects. In this

*Permanent address: Physics Department and Institute of Natural Sciences, Kyung Hee University, 1 Seochunli, Yoninsi, Kyunggido, Korea.

 ©2001 The American Physical Society

paper we consider the effects of the Coulomb interaction and surface tension by considering a uniform spherical finite nuclear system. Various dynamic approaches exist for the study of the Coulomb interaction and surface effects in asymmetric nuclear system. For example, Ref. [10] is an investigation of the role of the Coulomb interaction on the growth of unstable modes. These authors use a linearized Vlasov equation as a semiclassical approximation to a quantal random phase approximation (RPA) approach and also consider results from a RPA study. The growth rates of unstable modes were also studied in Refs. [11,12] using a Skyrme interaction. The calculation of Ref. [11] is based on the Vlasov equation while that of Ref. [12] uses a RPA method. References [10,12] show that the Coulomb interaction reduces the chemical instability region, an effect which is also found here. However, a new effect appears in this work which is the appearance of a new pair of binodal points at low pressure and large proton fraction which is discussed.

In Sec. II, the main equations for the thermodynamic properties of hot nuclear matter in mean field theory are developed as a function of density $\rho$, temperature $T$, and proton fraction $y$ or neutron fraction $(1-y)$. These include the pressure and chemical potentials, both neutron $\mu_n$ and proton $\mu_p$, where phase equilibrium requires equality of the proton chemical potential between the two phases and similarly equality of the neutron chemical potentials at a given temperature and $P$. At fixed $T$ and $P$, $\rho$ and $y$ are not independent and we use this connection to simplify the analysis. This can be done because we use a Skyme interaction which leads to a series of simple closed form expressions, thereby making the analysis of the thermodynamic properties of asymmetric nuclear matter much easier. Section III contains the results of calculations performed using the equations developed in Sec. II. Conclusions are given in Sec. IV.

## II. PHASE TRANSITION IN MEAN FIELD THEORY

For phase transitions we look at the pressure $P$ and chemical potentials $\mu_q$ for each component of a multicomponent system (neutron and proton, for example) as functions of temperature $T$ and densities $\rho_q$ of the constituents. These quantities can be obtained once we know the total energy functional $E$ as a function of the densities $\rho_q$ at a given temperature $T$.

At a given temperature $T=1/\beta$, the constituents are distributed in phase space according to the Wigner function $f$ as

$$f(\vec{r},\vec{p})=\sum_q f_q(\vec{r},\vec{p}),\quad f_q(\vec{r},\vec{p})=\frac{\gamma}{h^3}\tilde{f}_q(\vec{r},\vec{p})=\frac{\gamma}{h^3}\frac{1}{e^{\beta(\epsilon_q-\mu_q)}+1}, \tag{1}$$

where the spin degeneracy $\gamma=2$ and $\epsilon_q$ and $\mu_q$ are the single-particle energy and the chemical potential of particle type $q$. Then the particle density $\rho$ becomes

$$\rho(\vec{r})=\sum_q \rho_q(\vec{r}),\quad \rho_q(\vec{r})=\int d^3p f_q(\vec{r},\vec{p}), \tag{2}$$

$$A=\sum_q N_q=\int d^3r\rho(\vec{r}),\quad N_q=\int d^3r\rho_q(\vec{r})=\int d^3r\int d^3p f_q(\vec{r},\vec{p}), \tag{3}$$

and the total energy is

$$E=\int d^3r\mathcal{E}(\vec{r})=\int d^3r\int d^3p\frac{p^2}{2m}f(\vec{r},\vec{p})+\int d^3rU(\vec{r})=\int d^3r[\mathcal{E}_K(\vec{r})+U(\vec{r})], \tag{4}$$

with the potential energy density $U(\vec{r})$ and the kinetic energy density $\mathcal{E}_K(\vec{r})$. These, in turn, give self-consistent equations for $\mu_q$ (or $p_{Fq}$) in a mean field theory for fixed $T$ and $N_q$,

$$\epsilon_q=\frac{\delta E}{\delta f_q}=\frac{\delta\mathcal{E}(\vec{r})}{\delta f_q(\vec{r},\vec{p})}=\frac{p^2}{2m}+\frac{\delta U}{\delta f_q}=\frac{p^2}{2m}+u_q(\vec{r},\vec{p}), \tag{5}$$

$$\mu_q=\epsilon_q|_{p=p_{Fq}}=\frac{p_{Fq}^2}{2m}+u_q(\vec{r},\vec{p}_{Fq}), \tag{6}$$

where we define $p_{Fq}$ in Eq. (6) and consider it as an effective Fermi momentum at $T$ of particle $q$, which is the momentum associated with the chemical potential, and $u_q=\delta U/\delta f_q$ is the single-particle potential of particle $q$ which may be momentum dependent in general.

The pressure $P$ can be defined dynamically from the total momentum conservation law $(d/dt)[\int d^3r\int d^3p\vec{p}f]=-\int d^3r\vec{\nabla}_r\cdot\vec{\vec{\Pi}}=0$ using the Vlasov equation [13]

$$\frac{\partial f_q}{\partial t}+(\vec{\nabla}_p\epsilon_q)\cdot(\vec{\nabla}_r f_q)-(\vec{\nabla}_r\epsilon_q)\cdot(\vec{\nabla}_p f_q)=0 \tag{7}$$

or more generally from hydrodynamic consideration of time dependent Hartree-Fock in phase space [14]:

$$\vec{\nabla}_r\cdot\vec{\vec{\Pi}}=-\frac{d}{dt}\left[\int d^3p\vec{p}\sum_q f_q(\vec{r},\vec{p})\right]=-\sum_q\int d^3p\vec{p}\left(\frac{\partial f_q}{\partial t}\right)=\sum_q\int d^3p\vec{p}\ \vec{\nabla}_r\cdot[(\vec{\nabla}_p\epsilon_q)f_q]+\sum_q\int d^3pf_q(\vec{\nabla}_r\epsilon_q)\cdot(\vec{\nabla}_p\vec{p}). \tag{8}$$

Using $\Sigma_q(\vec{\nabla}_r\epsilon_q)f_q=\Sigma_q\vec{\nabla}_r(\epsilon_q f_q)-\Sigma_q\epsilon_q\vec{\nabla}_r f_q=\Sigma_q\vec{\nabla}_r(\epsilon_q f_q)-\vec{\nabla}_r\mathcal{E}$, the dynamical pressure tensor $\Pi_{ij}$ becomes

$$\begin{aligned}\Pi_{ij}&=\sum_q\int d^3pp_j(\nabla_p^i\epsilon_q)f_q+\delta_{ij}\left[\int d^3p\sum_q\epsilon_q f_q-\mathcal{E}\right]\\&=\sum_q\int d^3pp_j\nabla_p^i\left(\frac{\delta\mathcal{E}}{\delta f_q}\right)f_q+\delta_{ij}\left[\sum_q\int d^3p\left(\frac{\delta\mathcal{E}}{\delta f_q}\right)f_q-\mathcal{E}\right]\\&=\sum_q\int d^3pp_j\left[\frac{p_i}{m}+\nabla_p^i\left(\frac{\delta U}{\delta f_q}\right)\right]f_q+\delta_{ij}\left[\sum_q\int d^3p\left(\frac{\delta U}{\delta f_q}\right)f_q-U\right].\end{aligned} \tag{9}$$

For a momentum-independent potential, this becomes

$$\Pi_{ij}=\sum_q\int d^3p\frac{p_ip_j}{m}f_q+\delta_{ij}\left[\sum_q\left(\frac{\delta U}{\delta\rho_q}\right)\rho_q-U\right]=\int d^3p\sum_q\frac{p_ip_j}{m}f_q+\delta_{ij}\sum_q\rho_q^2\frac{\delta(U/\rho_q)}{\delta\rho_q}. \tag{10}$$

The diagonal elements are

$$P=\Pi_{ii}=\sum_q\int d^3p\frac{p_i^2}{m}f_q+\sum_q\frac{\delta U}{\delta\rho_q}\rho_q-U=P_K+\sum_q u_q\rho_q-U=P_K+P_P, \tag{11}$$

where $P_K=\int d^3p(p_i^2/m)f$ and $P_P=\Sigma_q u_q\rho_q-U$ are the kinetic pressure and interaction (potential) pressure, respectively. In equilibrium $P$ can also be obtained by minimizing the total energy as a function of volume, holding the number of particles fixed:

$$P=\Pi_{ii}=-\frac{d(E/A)}{dV}=\rho^2\frac{d(\mathcal{E}/\rho)}{d\rho} \tag{12}$$

for a single-component uniform system.

From the distribution $\tilde{f}_q$ of Eq. (1), the entropy $S$ can be obtained as

$$S=\sum_q S_q=\int d^3r\mathcal{S}=\int d^3r\sum_q\mathcal{S}_q, \tag{13}$$

$$\begin{aligned}\mathcal{S}_q&=-\frac{\gamma}{h^3}\int d^3p[\tilde{f}_q\ln\tilde{f}_q+(1-\tilde{f}_q)\ln(1-\tilde{f}_q)]\\&=\frac{\gamma}{h^3}\int d^3p\frac{1}{3}\vec{p}\cdot(\vec{\nabla}_p\tilde{f}_q)\ln\left[\frac{\tilde{f}_q}{1-\tilde{f}_q}\right]\\&=\frac{\gamma}{h^3}\int d^3p\frac{1}{3}\vec{p}\cdot(\vec{\nabla}_p\tilde{f}_q)\beta(\mu_q-\epsilon_q),\end{aligned} \tag{14}$$

using $\vec{\nabla}_p\cdot(\vec{p}g)=3g+\vec{p}\cdot\vec{\nabla}_p g$. The $\mathcal{S}_q$ becomes, by partial integration [15],

$$\begin{aligned}\mathcal{S}_q&=\beta\int d^3p\frac{1}{3}\vec{p}\cdot\vec{\nabla}_p[(\mu_q-\epsilon_q)f_q]\\&\quad-\beta\int d^3p\frac{1}{3}\vec{p}\cdot\vec{\nabla}_p(\mu_q-\epsilon_q)f_q\\&=\beta\int d^3p(\epsilon_q-\mu_q)f_q+\beta\int d^3p\frac{\vec{p}\cdot\vec{\nabla}_p\epsilon_q}{3}f_q\\&=\beta\int d^3p\,\epsilon_q f_q+\beta\int d^3p\frac{\vec{p}\cdot\vec{\nabla}_p\epsilon_q}{3}f_q-\beta\mu_q\int d^3pf_q.\end{aligned} \tag{15}$$

In equilibrium thermodynamics, the thermodynamic grand potential $\Omega$, the Helmholtz free energy $F$, and the Gibb's free energy $G$ are

$$\begin{aligned}\Omega&=-\int d^3rP\\&=-\frac{1}{\beta}\ln\mathrm{Tr}\exp\left[-\beta\left(\hat{H}-\sum_q\mu_q\hat{N}_q\right)\right]\\&=F-G=E-TS-\sum_q\mu_qN_q,\end{aligned} \tag{16}$$

$$F=\int d^3r\mathcal{F}=-\frac{1}{\beta}\ln\mathrm{Tr}\,e^{-\beta\hat{H}}=E-TS=T\int Ed\beta, \tag{17}$$

$$G=\int d^3r\mathcal{G}=\frac{1}{\beta}\ln \mathrm{Tr}\exp\left(\beta\sum_q \mu_q\hat{N}\right)$$

$$=\sum_q \mu_q N_q$$

$$=\int d^3r\sum_q \mu_q\rho_q. \tag{18}$$

Comparing Eq. (15) with Eq. (9) for diagonal elements using $p_i\nabla_p^i=\frac{1}{3}\vec{p}\cdot\vec{\nabla}_p$ (isotropic condition in momentum, $p_i^2=\frac{1}{3}p^2$),

$$T\mathcal{S}=\mathcal{E}+P-\sum_q \mu_q\rho_q=\mathcal{E}-\mathcal{F}=\mathcal{E}_K+P_K-\sum_q (\mu_q-u_q)\rho_q, \tag{19}$$

$$\mathcal{F}=\sum_q \mu_q\rho_q-P=\sum_q (\mu_q-u_q)\rho_q-P_K+U, \tag{20}$$

$$\mathcal{G}=\sum_q \mathcal{G}_q=\sum_q \mu_q\rho_q. \tag{21}$$

The entropy can also be found from $dQ=TdS=CdT$:

$$\Delta S=\int\frac{dQ}{T}=\int\frac{CdT}{T}=\int\frac{1}{T}\frac{dE}{dT}dT$$

$$=\int\beta\frac{dE}{d\beta}d\beta=\beta E-\int E d\beta=\beta(E-F). \tag{22}$$

The pressure and the chemical potential are also related to the free energy $F$ as

$$P=-\left.\frac{\partial F}{\partial V}\right|_{T,A}=-\left.\frac{\partial\Omega}{\partial V}\right|_{T,A}, \tag{23}$$

$$\mu=\left.\frac{\partial F}{\partial A}\right|_{T,V}. \tag{24}$$

The specific heat capacity is given by, from the entropy per particle, $\mathcal{S}/\rho$,

$$c_P=T\left(\frac{\partial\mathcal{S}/\rho}{\partial T}\right)_P \quad\text{or}\quad c_V=T\left(\frac{\partial\mathcal{S}/\rho}{\partial T}\right)_V. \tag{25}$$

To study the caloric curve or the specific heat we look at the energy per particle $\mathcal{E}/\rho$ and the entropy per particle $\mathcal{S}/\rho$.

For multiphase multicomponent systems, the phase transition of each component can occur at different conditions such as temperature or pressure. However, in general we can treat all different possible combinations of phases of each component in the multicomponent system as different phases of the system. (As an example suppose we have a system of particles of type $p$ and particles of type $n$, each having a liquid-gas phase transition but at different temperatures. Then the system can be in one of the following four phases: a phase of liquid $p$ and liquid $n$, a phase of liquid $p$ and gas $n$, a phase of gas $p$ and liquid $n$, or a phase of gas $p$ and gas $n$.) Then, to separate each phase of the multicomponent system, we can use the volume fraction $\lambda_i$ of $i$ phase of the total volume $V$ which depends on $T$,

$$\lambda_i=V_i/V \quad\text{with}\quad \sum_i \lambda_i=1, \tag{26}$$

$$\rho_q=\sum_i \lambda_i\rho_q^i, \tag{27}$$

$$\mathcal{O}(\rho_q,T)=\sum_i \lambda_i\mathcal{O}(T,\rho_q^i), \tag{28}$$

where $\mathcal{O}$ is any observable per unit volume. Within the spinodal instability region, there is no equilibrated phase. Two or multiple phases can coexist when the pressure $P$ and each chemical potential $\mu_q$ are all the same among these phases, i.e.,

$$P_i=P_j, \tag{29}$$

$$\mu_q^i=\mu_q^j, \tag{30}$$

with different values of $\rho_q^i$ and $\rho_q^j$ for all $i$ and $j$. At the critical point,

$$\frac{\partial P}{\partial\rho_q}=\frac{\partial^2 P}{\partial\rho_q^2}=0, \tag{31}$$

$$\frac{\partial\mu_q}{\partial\rho_q}=\frac{\partial^2\mu_q}{\partial\rho_q^2}=0. \tag{32}$$

Spinodal instability occurs when $\partial P/\partial\rho_q$ is negative.

Once the potential energy $U$ in Eq. (4) is known, then the possibility of a phase transition of the system can be studied using Eqs. (1)–(25). The potential energy $U$ determines $\epsilon_q$ and $\mu_q$ and the potential energy part of $E$ and $P$. Then for fixed $T$ and $N_q$, the Wigner function $f$ and $p_{Fq}$ are determined and thus the kinetic terms of $E$, $\mu_q$, and $P$. Using these results, the entropy $\mathcal{S}$ and $c_P$ can be determined. Relativistic mean field theory is used for the interaction in Ref. [7]. The role of the Coulomb interaction and surface energy or the finite size effect of a nucleus are neglected in Ref. [7] but will be included in the approach developed here. Their result shows that the neutron evaporates first as the energy of the system increases, leaving more charge concentrated in liquid phase. In this approach the coupled equations of nucleons and mesons lead to a highly nonlinear system and thus the equation of state can be obtained only through a self-consistent iterative way. These problems may be simplified by using a nonrelativistic zero-range Skyrme interaction of

$$v_{12}=t_0(1+x_0P^\sigma)\delta(\vec{r}_1-\vec{r}_2)$$

$$+\frac{t_3}{6}(1+x_3P^\sigma)\rho^\alpha\left(\frac{\vec{r}_1+\vec{r}_2}{2}\right)\delta(\vec{r}_1-\vec{r}_2). \tag{33}$$

TABLE I. Parameter sets for the Skyrme interaction [1,16].

| Force | $\alpha$ | $t_0$ (MeV fm$^3$) | $x_0$ | $t_3$ (MeV fm$^{3(1+\alpha)}$) | $x_3$ |
|---|---|---|---|---|---|
| PRC45 | 1 | $\frac{4}{3}C_1=-1089.0$ | 1/2 | $\frac{16}{\alpha+2}C_2=17480.4$ | $-1/2$ |
| ZR1 | 1 | $-1003.9$ | 0.0, 0.2, 0.5 | 13287.2 | 1.0 |
| ZR2 | 2/3 | $-1192.2$ | 0.0, 0.2, 0.5 | 11041.0 | 1.0 |
| ZR3 | 0.1 | $-4392.2$ | 0.0, 0.2, 0.5 | 26967.3 | 1.0 |

For a nuclear system of proton ($\rho_p$) and neutron ($\rho_n$), this gives the local potential energy density as

$$U(\rho_q)=\frac{t_0}{2}\left(1+\frac{x_0}{2}\right)\rho^2-\frac{t_0}{2}\left(\frac{1}{2}+x_0\right)\sum_q \rho_q^2 + \frac{t_3}{12}\left(1+\frac{x_3}{2}\right)\rho^{\alpha+2}-\frac{t_3}{12}\left(\frac{1}{2}+x_3\right)\rho^{\alpha} \times\sum_q \rho_q^2+C\rho^{\beta}\rho_p^2+C_s\rho^{\eta}. \tag{34}$$

Here $C\rho^{\beta}=(4\pi/5)e^2R^2$ and $C_s\rho^{\eta}=4\pi R^2\sigma(\rho)/V=[(4\pi r_0^2\sigma)/V^{1/3}]\rho^{2/3}$ when we approximate the Coulomb and surface effects as coming from a finite uniform sphere of radius $R=r_0A^{1/3}$ with total charge $Z$ ($U_C=\frac{3}{5}e^2Z^2/RV$). This way of handling the Coulomb interaction and surface tension is a simplification of a very difficult problem. Despite the limitation of the geometry used to calculate the Coulomb interaction, we feel that the results obtained from it will be instructive and also very useful in accessing its importance on the phase transition in two-component systems. The typical values for the force parameters are given in Table I. For a symmetric nucleus, $N=Z$, $\rho_q=\rho/2$, and thus

$$U(\rho)=\frac{3}{8}t_0\rho^2+\frac{3}{48}t_3\rho^{\alpha+2}+C\rho^{\beta}\rho_p^2+C_s\rho^{\eta}. \tag{35}$$

This potential energy determines the interaction-dependent terms of $\mathcal{E}$, $P$, $\epsilon_q$, and $\mu_q$ which depend on densities without explicit $T$ dependence.

For a momentum-independent potential energy as in Eq. (34), $\epsilon_q-\mu_q=(p^2-p_{Fq}^2)/(2m)$ is independent of the potential and

$$f_q(\vec{r},\vec{p})=\frac{\gamma}{h^3}\tilde{f}_q(\vec{r},\vec{p}),\quad \tilde{f}_q(\vec{r},\vec{p})=\frac{1}{e^{\beta(p^2-p_{Fq}^2)/(2m)}+1}. \tag{36}$$

Thus we can evaluate the kinetic terms in $\mathcal{E}$, $P$, and $\mu_q$ which are functions of $T$ and $p_{Fq}$. Defining the Fermi integral $F_\alpha(\eta)$,

$$F_\alpha(\eta_q)=\int_0^\infty\frac{x^\alpha}{1+e^{x-\eta_q}}dx=\left(\frac{\lambda^2}{4\pi\hbar^2}\right)^{\alpha+1}\int_0^\infty\frac{2p^{2\alpha+1}dp}{1+e^{\beta p^2/2m-\eta_q}}, \tag{37}$$

$$\eta_q=\beta(\mu_q-u_q)=\beta p_{Fq}^2/(2m)=p_{Fq}^2/(2mT)=\ln z_q, \tag{38}$$

$$\lambda=\sqrt{2\pi\hbar^2/mT}, \tag{39}$$

we can write, for $f(\vec{r},\vec{p})=f(\vec{r},p)$,

$$\rho_q=\int d^3p f_q(\vec{r},\vec{p})=\frac{\gamma}{h^3}\int d^3p\frac{1}{e^{\beta(p^2-p_{Fq}^2)/(2m)}+1} =\lambda^{-3}\frac{2\gamma}{\sqrt{\pi}}F_{1/2}(\eta_q), \tag{40}$$

$$\epsilon_{Fq}\equiv\frac{\hbar^2}{2m}\left(\frac{6\pi^2}{\gamma}\rho_q\right)^{2/3}, \tag{41}$$

$$\mathcal{E}_{Kq}=\frac{3}{2}P_{Kq}=\int d^3p\frac{p^2}{2m}f_q(\vec{r},\vec{p}) =\frac{\gamma}{h^3}\int d^3p\frac{p^2}{2m}\frac{1}{e^{\beta(p^2-p_{Fq}^2)/(2m)}+1} =\frac{4\gamma\hbar^2\sqrt{\pi}}{m}\lambda^{-5}F_{3/2}(\eta_q) =\frac{1}{\beta}\frac{2\gamma}{\sqrt{\pi}}\lambda^{-3}F_{3/2}(\eta_q). \tag{42}$$

Here $\epsilon_{Fq}$ is the chemical potential at absolute zero or Fermi energy and $p_{Fq}$ is the effective Fermi momentum at $T$. The particle number $N_q=\int d^3r\rho_q(\vec{r})$ determines the effective Fermi momentum $p_{Fq}(\vec{r})$ or $\eta_q$ at $T$, in terms of density $\rho_q(\vec{r})$,

$$\eta_q(\rho_q,T)=\beta(\mu_q-u_q)=\beta\frac{p_{Fq}^2}{2m}=F_{1/2}^{-1}\left(\frac{\sqrt{\pi}}{2\gamma}\lambda^3\rho_q\right). \tag{43}$$

For multi- (two-)component systems with potential energy given by Eq. (34), for a given $\rho_q$ (or $p_{Fq}$) and $T$,

$$\mu_q(\rho_q,T)=T\eta_q(\rho_q,T)+t_0\left(1+\frac{x_0}{2}\right)\rho+\frac{t_3}{12}\left(1+\frac{x_3}{2}\right)(\alpha+2)\rho^{\alpha+1}-\frac{t_3}{12}\left(\frac{1}{2}+x_3\right)\alpha\rho^{\alpha+1}-t_0\left(\frac{1}{2}+x_0\right)\rho_q$$
$$+\frac{t_3}{12}\left(\frac{1}{2}+x_3\right)(\alpha-1)2\rho^{\alpha}\rho_q-\frac{t_3}{12}\left(\frac{1}{2}+x_3\right)2\alpha\rho^{\alpha-1}\rho_q^2+C\beta\rho^{\beta-1}\rho_p^2+2C\rho^{\beta}\rho_p\delta_{q,p}+\eta C_s\rho^{\eta-1}, \quad (44)$$

$$P(\rho_q,T)=\sum_q\frac{2}{3}\mathcal{E}_{Kq}(\rho_q,T)+\frac{t_0}{2}\left(1+\frac{x_0}{2}\right)\rho^2+\frac{t_3}{12}\left(1+\frac{x_3}{2}\right)(\alpha+1)\rho^{\alpha+2}-\frac{t_0}{2}\left(\frac{1}{2}+x_0\right)\sum_q\rho_q^2$$
$$-\frac{t_3}{12}\left(\frac{1}{2}+x_3\right)(\alpha+1)\rho^{\alpha}\sum_q\rho_q^2+C(\beta+1)\rho^{\beta}\rho_p^2+C_s(\eta-1)\rho^{\eta}, \quad (45)$$

$$\mathcal{E}(\rho_q,T)=\sum_q\mathcal{E}_{Kq}(\rho_q,T)+\frac{t_0}{2}\left(1+\frac{x_0}{2}\right)\rho^2-\frac{t_0}{2}\left(\frac{1}{2}+x_0\right)\sum_q\rho_q^2+\frac{t_3}{12}\left(1+\frac{x_3}{2}\right)\rho^{\alpha+2}$$
$$-\frac{t_3}{12}\left(\frac{1}{2}+x_3\right)\rho^{\alpha}\sum_q\rho_q^2+C\rho^{\beta}\rho_p^2+C_s\rho^{\eta}, \quad (46)$$

$$T\mathcal{S}(\rho_q,T)=\sum_q\frac{5}{3}\mathcal{E}_{Kq}(\rho_q,T)-\sum_q(\mu_q-u_q)\rho_q=\sum_q\frac{5}{3}\mathcal{E}_{Kq}(\rho_q,T)-T\sum_q\eta_q(\rho_q,T)\rho_q, \quad (47)$$

$$c_P(\rho_q,T)=\frac{dQ/A}{dT}=T\left(\frac{\partial\mathcal{S}/\rho}{\partial T}\right)_P \text{ or } c_V(\rho_q,T)=T\left(\frac{\partial\mathcal{S}/\rho}{\partial T}\right)_V. \quad (48)$$

Once we evaluate $F_{1/2}(\eta)$ and $F_{3/2}(\eta)$, or more directly $\eta=F_{1/2}^{-1}(\chi)$ and $F_{3/2}(\eta)$, we can evaluate various thermodynamic quantities in terms of $\rho_q$ and $T$.

For the low temperature and high density limit, $\lambda^3\rho$ large, i.e., when the average de Broglie thermal wavelength $\lambda$ is larger than the average interparticle separation $\rho^{-1/3}$, we can use nearly degenerate (Fermi gas) approximations [17] for $F_{1/2}$ to obtain

$$\eta_q(\rho_q,T)=\beta(\mu_q-u_q)=\beta\frac{p_{Fq}^2}{2m}=F_{1/2}^{-1}\left(\frac{\sqrt{\pi}}{2\gamma}\lambda^3\rho_q\right)=\epsilon_{Fq}\left[1-\frac{\pi^2}{12}\left(\frac{T}{\epsilon_{Fq}}\right)^2+\cdots\right]$$
$$=\frac{\hbar^2}{2m}\left(\frac{6\pi^2}{\gamma}\right)^{2/3}\left[\rho_q^{2/3}-\frac{\pi^2m^2}{3\hbar^4}\left(\frac{\gamma}{6\pi^2}\right)^{4/3}T^2\rho_q^{-2/3}+\cdots\right], \quad (49)$$

$$\mathcal{E}_{Kq}(\rho_q,T)=\frac{2\gamma}{\beta\sqrt{\pi}}\lambda^{-3}F_{3/2}(\eta_q)=\frac{3}{5}\rho_q\epsilon_{Fq}\left[1+\frac{5\pi^2}{12}\left(\frac{T}{\epsilon_{Fq}}\right)^2+\cdots\right]$$
$$=\frac{3\hbar^2}{10m}\left(\frac{6\pi^2}{\gamma}\right)^{2/3}\left[\rho_q^{5/3}+\frac{5\pi^2m^2}{3\hbar^4}\left(\frac{\gamma}{6\pi^2}\right)^{4/3}T^2\rho_q^{1/3}+\cdots\right]. \quad (50)$$

In the other limit where $\lambda^3\rho$ is small, we have a nearly nondegenerate Fermi gas (classical ideal gas) and the resulting equations are given by an ideal gas in leading order with higher order corrections [17] as

$$\eta_q(\rho_q,T)=\beta(\mu_q-u_q)=\ln\left[\frac{\rho_q\lambda^3}{\gamma}\left(1+\frac{1}{2\sqrt{2}}\frac{\rho_q\lambda^3}{\gamma}+\cdots\right)\right]\approx\ln\left(\frac{\rho_q\lambda^3}{\gamma}\right)+\frac{1}{2\sqrt{2}}\left(\frac{\rho_q\lambda^3}{\gamma}\right), \quad (51)$$

$$\mathcal{E}_{Kq}(\rho_q,T)=\frac{3}{2}P_{Kq}=\frac{3}{2}\rho_qT\left[1+\frac{1}{2^{5/2}}\frac{\rho_q\lambda^3}{\gamma}+\left(\frac{1}{8}-\frac{2}{3^{5/2}}\right)\left(\frac{\rho_q\lambda^3}{\gamma}\right)^2+\cdots\right]. \quad (52)$$

For a nuclear system with protons and neutrons with the interaction given by Eq. (34), the nondegenerate Fermi gas limit of Eqs. (51) and (52) leads to the following set of equations:

$$\mu_q(\rho,y,T)=T\ln\left[\left(\frac{\lambda^3}{\gamma}\right)\rho_q\right]+\frac{T}{2\sqrt{2}}\left(\frac{\lambda^3}{\gamma}\right)\rho_q+t_0\left(1+\frac{x_0}{2}\right)\rho+\frac{t_3}{12}\left(1+\frac{x_3}{2}\right)(\alpha+2)\rho^{\alpha+1}-\frac{t_3}{12}\left(\frac{1}{2}+x_3\right)\alpha\rho^{\alpha+1}-t_0\left(\frac{1}{2}+x_0\right)\rho_q$$
$$+\frac{t_3}{12}\left(\frac{1}{2}+x_3\right)(\alpha-1)2\rho^{\alpha}\rho_q-\frac{t_3}{12}\left(\frac{1}{2}+x_3\right)2\alpha\rho^{\alpha-1}\rho_q^2+C\beta\rho^{\beta-1}\rho_p^2+2C\rho^{\beta}\rho_p\delta_{q,p}+\eta C_s\rho^{\eta-1}$$
$$=T\ln\left\{\left(\frac{\lambda^3}{\gamma}\right)\left[\frac{\rho}{2}\pm(2y-1)\left(\frac{\rho}{2}\right)\right]\right\}+\frac{T}{2\sqrt{2}}\left(\frac{\lambda^3}{\gamma}\right)\left[\frac{\rho}{2}\pm(2y-1)\frac{\rho}{2}\right]+\frac{3}{4}t_0\rho\mp\left(\frac{1}{2}+x_0\right)t_0(2y-1)\left(\frac{\rho}{2}\right)+\frac{(\alpha+2)}{16}$$
$$\times t_3\rho^{\alpha+1}-\frac{1}{6}\left(\frac{1}{2}+x_3\right)t_3\left[\alpha(2y-1)^2\left(\frac{\rho}{2}\right)^2\pm(2y-1)\left(\frac{\rho}{2}\right)\rho\right]\rho^{\alpha-1}+\frac{1}{4}C[\beta+2(1\pm1)]\rho^{\beta+1}$$
$$+C\left[(\beta+1\pm1)(2y-1)\left(\frac{\rho}{2}\right)\rho+\beta(2y-1)^2\left(\frac{\rho}{2}\right)^2\right]\rho^{\beta-1}+\eta C_s\rho^{\eta-1}, \tag{53}$$

$$P(\rho,y,T)=T\rho+\frac{T}{2\sqrt{2}}\left(\frac{\lambda^3}{\gamma}\right)\left(\frac{\sum_q\rho_q^2}{2}\right)+\frac{t_0}{2}\left(1+\frac{x_0}{2}\right)\rho^2+\frac{t_3}{12}\left(1+\frac{x_3}{2}\right)(\alpha+1)\rho^{\alpha+2}-\frac{t_0}{2}\left(\frac{1}{2}+x_0\right)\sum_q\rho_q^2$$
$$-\frac{t_3}{12}\left(\frac{1}{2}+x_3\right)(\alpha+1)\rho^{\alpha}\sum_q\rho_q^2+C(\beta+1)\rho^{\beta}\rho_p^2+C_s(\eta-1)\rho^{\eta}$$
$$=T\rho+\frac{3}{8}t_0\rho^2+\frac{(\alpha+1)}{16}t_3\rho^{\alpha+2}+\frac{T}{2\sqrt{2}}\left(\frac{\lambda^3}{\gamma}\right)\left(\frac{\rho}{2}\right)^2+\frac{(\beta+1)}{4}C\rho^{\beta+2}+(\eta-1)C_s\rho^{\eta}$$
$$-\left[t_0\left(\frac{1}{2}+x_0\right)+\left(\frac{\alpha+1}{6}\right)t_3\left(\frac{1}{2}+x_3\right)\rho^{\alpha}-\frac{T}{2\sqrt{2}}\left(\frac{\lambda^3}{\gamma}\right)-(\beta+1)C\rho^{\beta}\right](2y-1)^2\left(\frac{\rho}{2}\right)^2+(\beta+1)C\rho^{\beta+1}(2y-1)$$
$$\times\left(\frac{\rho}{2}\right), \tag{54}$$

$$\mathcal{E}(\rho,y,T)=\frac{3}{2}T\rho+\frac{3}{2}\frac{T}{2\sqrt{2}}\left(\frac{\lambda^3}{\gamma}\right)\left(\frac{\sum_q\rho_q^2}{2}\right)+\frac{t_0}{2}\left(1+\frac{x_0}{2}\right)\rho^2-\frac{t_0}{2}\left(\frac{1}{2}+x_0\right)\sum_q\rho_q^2+\frac{t_3}{12}\left(1+\frac{x_3}{2}\right)\rho^{\alpha+2}$$
$$-\frac{t_3}{12}\left(\frac{1}{2}+x_3\right)\rho^{\alpha}\sum_q\rho_q^2+C\rho^{\beta}\rho_p^2+C_s\rho^{\eta}$$
$$=\frac{3}{2}T\rho+\frac{3}{8}t_0\rho^2+\frac{1}{16}t_3\rho^{\alpha+2}+\frac{3}{2}\frac{T}{2\sqrt{2}}\left(\frac{\lambda^3}{\gamma}\right)\left(\frac{\rho}{2}\right)^2+\frac{1}{4}C\rho^{\beta+2}+C_s\rho^{\eta}$$
$$-\left[t_0\left(\frac{1}{2}+x_0\right)+\left(\frac{1}{6}\right)t_3\left(\frac{1}{2}+x_3\right)\rho^{\alpha}-\frac{3}{2}\frac{T}{2\sqrt{2}}\left(\frac{\lambda^3}{\gamma}\right)-C\rho^{\beta}\right](2y-1)^2\left(\frac{\rho}{2}\right)^2+C\rho^{\beta+1}(2y-1)\left(\frac{\rho}{2}\right), \tag{55}$$

$$T\mathcal{S}(\rho,y,T)=\frac{5}{2}T\rho-T\sum_q\rho_q\ln\left(\frac{\lambda^3}{\gamma}\rho_q\right)+\frac{T}{2\sqrt{2}}\left(\frac{\lambda^3}{\gamma}\right)\left(\frac{\sum_q\rho_q^2}{4}\right)$$
$$=T\rho\left[\frac{5}{2}-y\ln\left(\frac{\lambda^3}{\gamma}y\rho\right)-(1-y)\ln\left(\frac{\lambda^3}{\gamma}(1-y)\rho\right)\right]+\frac{T}{2\sqrt{2}}\left(\frac{\lambda^3}{\gamma}\right)\frac{[1+(2y-1)^2]}{2}\left(\frac{\rho}{2}\right)^2. \tag{56}$$

Here, for the proton density ($\rho_p$) and neutron density ($\rho_n$), we defined

$$\rho=\rho_p+\rho_n, \quad \rho_3=\rho_p-\rho_n=(2y-1)\rho, \quad y=\rho_p/\rho,$$

$$\rho_p=\tfrac{1}{2}(\rho+\rho_3)=y\rho, \quad \rho_n=\tfrac{1}{2}(\rho-\rho_3)=(1-y)\rho,$$

$$\sum_q \rho_q^2=\frac{1}{2}(\rho^2+\rho_3^2)=\frac{[1+(2y-1)^2]}{2}\rho^2=[1+2y(y-1)]\rho^2,$$

$$\sum_q \rho_q^3=\frac{1}{4}\rho(\rho^2+3\rho_3^2)=\frac{[1+3(2y-1)^2]}{4}\rho^3=[1+3y(y-1)]\rho^3. \tag{57}$$

The $\pm$ in $\mu_q$ stands $+$ for $q=$ proton and $-$ for neutron. Equation (54) shows that, for $x_3\neq -1/2$ and $C\neq 0$, the $P(\rho)$ curve for different values of $y$ at fixed $T$ may cross at some $\rho$. Moreover, the minimum pressure for a given $T$ and $\rho$ [i.e., $(\partial P/\partial y)_{\rho,T}=0$] occurs at $y\neq 0.5$ due to the Coulomb effect. These results were not seen in Ref. [7]. Also Eq. (55) shows that, for $x_3=-1/2$ and $C=0$, the symmetry energy per nucleon is increasing proportionally to the density $\rho$, a feature similar to that in Ref. [7]. However, for $x_3\neq -1/2$, the symmetry energy initially starts to increase with $\rho$ but then begins to decrease with increasing $\rho$. This bending of the symmetry energy is related to the crossing of $P(\rho)$ curves of different $y$ values for a fixed $T$.

For a constant $T$ and constant $P$, $\rho$ and $y$ are not independent. The pressure $P$ of Eq. (54) is a second-order polynomial of $(2y-1)(\rho/2)$, and thus we have, for the range of $0\leqslant y\leqslant 1/2$,

$$\begin{aligned}(2y-1)=&\frac{(\beta+1)C\rho^\beta}{\left(\frac{1}{2}+x_0\right)t_0+\left(\frac{\alpha+1}{6}\right)\left(\frac{1}{2}+x_3\right)t_3\rho^\alpha-(\beta+1)C\rho^\beta-\frac{T}{2\sqrt{2}}\left(\frac{\lambda^3}{\gamma}\right)}\\ &\mp\frac{2}{\rho}\left[\left(\frac{(\beta+1)C\rho^\beta}{\left(\frac{1}{2}+x_0\right)t_0+\left(\frac{\alpha+1}{6}\right)\left(\frac{1}{2}+x_3\right)t_3\rho^\alpha-(\beta+1)C\rho^\beta-\frac{T}{2\sqrt{2}}\left(\frac{\lambda^3}{\gamma}\right)}\right)^2\left(\frac{\rho}{2}\right)^2\right.\\ &\left.+\frac{T\rho+\frac{3}{8}t_0\rho^2+\frac{(\alpha+1)}{16}t_3\rho^{\alpha+2}+\frac{(\beta+1)}{4}C\rho^{\beta+2}+(\eta-1)C_s\rho^\eta+\frac{T}{2\sqrt{2}}\left(\frac{\lambda^3}{\gamma}\right)\frac{\rho^2}{4}-P}{\left(\frac{1}{2}+x_0\right)t_0+\left(\frac{\alpha+1}{6}\right)\left(\frac{1}{2}+x_3\right)t_3\rho^\alpha-(\beta+1)C\rho^\beta-\frac{T}{2\sqrt{2}}\left(\frac{\lambda^3}{\gamma}\right)}\right]^{1/2}\end{aligned} \tag{58}$$

for a given density $\rho$. Here, $-1\leqslant(2y-1)\leqslant 0$, and thus a $+$ sign is allowed for the case that the first term is negative. Without the Coulomb interaction only the second term in the square root survives and $y(\rho)$ is a single-valued function of $\rho$ in the range of $0\leqslant y\leqslant 1/2$. The numerator of the second term in the square root is $P(\rho,y=1/2,T)-P(\rho,y,T)$, i.e., the negative of the pressure measured with respect to the pressure for a symmetric nuclear system. Notice here that $t_0$ is negative and $P(y)\geqslant P(y=1/2)$ for the potential without the Coulomb interaction [see Eq. (54)]. Since we are considering only $-1\leqslant(2y-1)\leqslant 0$, we have conditions of

$$\begin{aligned}0\leqslant&\pm\left[\frac{T\rho+\frac{3}{8}t_0\rho^2+\frac{(\alpha+1)}{16}t_3\rho^{\alpha+2}+\frac{(\beta+1)}{4}C\rho^{\beta+2}+(\eta-1)C_s\rho^\eta+\frac{T}{2\sqrt{2}}\left(\frac{\lambda^3}{\gamma}\right)\frac{\rho^2}{4}-P}{\left(\frac{1}{2}+x_0\right)t_0+\left(\frac{\alpha+1}{6}\right)\left(\frac{1}{2}+x_3\right)t_3\rho^\alpha-(\beta+1)C\rho^\beta-\frac{T}{2\sqrt{2}}\left(\frac{\lambda^3}{\gamma}\right)}\right]\\ \leqslant&\pm\left[\frac{2(\beta+1)C\rho^\beta}{\left(\frac{1}{2}+x_0\right)t_0+\left(\frac{\alpha+1}{6}\right)\left(\frac{1}{2}+x_3\right)t_3\rho^\alpha-(\beta+1)C\rho^\beta-\frac{T}{2\sqrt{2}}\left(\frac{\lambda^3}{\gamma}\right)}+1\right]\left(\frac{\rho}{2}\right)^2\end{aligned} \tag{59}$$

to have $0\leqslant y\leqslant 1/2$. Also the boundaries are related to the pressures at $y=1/2$ and $y=0$, respectively. Here the $\pm$ sign corresponds to the $\mp$ sign in Eq. (58). For nonzero $C$, there is a backbending in $y(\rho)$. This behavior is related to the choice of opposite sign for the square root term in Eq. (58) and double values of $y$ for a given $\rho$. To find the point of backbending,

we look at the $(\partial\rho/\partial y)_{T,P}=0$ point. At the same value of $y$ as the backbending point of $y(\rho)_{P,T}$, the pressure becomes smallest for a given $\rho$ and $T$, i.e., $(\partial P/\partial y)_{\rho,T}=0$ [see Eq. (60) below]. For $C=0$, there is no backbending since only the negative sign is allowed in Eq. (58). Using Eq. (58) we can find $\rho(P,y,T)$ and thus the energy and entropy as a function of pressure $P$, proton fraction $y$, and temperature $T$, i.e., $\mathcal{E}(P,y,T)$ and $\mathcal{S}(P,y,T)$. From these results we may study an isobaric phase transition. Since all the phases have the same pressure in the coexistence region, $\mu_q(P,y,T)$ may be used to find the coexistence region.

At fixed $T$ and $P$, only one of either $\rho$ or $y$ is the independent variable. Thus we have $\rho(P,y,T)$ and observables such as $P$, $\mathcal{E}/\rho$, $\mathcal{S}/\rho$ may have a discontinuity in $T$ or $y$ when $(\partial\rho/\partial T)_{y,P}$ or $(\partial\rho/\partial y)_{T,P}$ diverges. We can study the behavior of thermodynamic quantities at a fixed $P$ using $dP=0$ from Eq. (54),

$$
\begin{aligned}
dP=&\left\{\left[T\rho-\frac{T}{2\sqrt{2}}\left(\frac{\lambda^3}{\gamma}\right)\left(\frac{\sum_q \rho_q^2}{4}\right)\right]\right\}\frac{dT}{T}+\left\{\left[T\rho+\frac{T}{2\sqrt{2}}\left(\frac{\lambda^3}{\gamma}\right)\left(\sum_q \rho_q^2\right)\right]\right.\\
&+\left[t_0\left(1+\frac{x_0}{2}\right)\rho^2+\frac{t_3}{12}\left(1+\frac{x_3}{2}\right)(\alpha+1)(\alpha+2)\rho^{\alpha+2}-t_0\left(\frac{1}{2}+x_0\right)\left(\sum_q \rho_q^2\right)-\frac{t_3}{12}\left(\frac{1}{2}+x_3\right)(\alpha+1)(\alpha+2)\rho^{\alpha}\left(\sum_q \rho_q^2\right)\right.\\
&\left.\left.+C(\beta+1)(\beta+2)\rho^{\beta}\rho_p^2+C_s(\eta-1)\eta\rho^{\eta}\right]\right\}\frac{d\rho}{\rho}\\
&-\left\{\left[t_0\left(\frac{1}{2}+x_0\right)+\left(\frac{\alpha+1}{6}\right)t_3\left(\frac{1}{2}+x_3\right)\rho^{\alpha}-(\beta+1)C\rho^{\beta}-\frac{T}{2\sqrt{2}}\left(\frac{\lambda^3}{\gamma}\right)\right]\left(\frac{\rho\rho_3}{4}\right)+(\beta+1)C\rho^{\beta}\left(\frac{\rho}{2}\right)^2\right\}4dy\\
=&\left\{\left[\rho-\frac{1}{2}\frac{1}{2\sqrt{2}}\left(\frac{\lambda^3}{\gamma}\right)\left(\frac{\rho}{2}\right)^2-\frac{1}{2}\frac{1}{2\sqrt{2}}\left(\frac{\lambda^3}{\gamma}\right)(2y-1)^2\left(\frac{\rho}{2}\right)^2\right]\right\}dT+\left\{\left[T+2\tilde{b}_2\rho+(\alpha+2)\tilde{b}_3\rho^{\alpha+1}+\frac{T}{2\sqrt{2}}\left(\frac{\lambda^3}{\gamma}\right)\left(\frac{\rho}{2}\right)\right.\right.\\
&\left.+(\beta+2)\tilde{b}_C\rho^{\beta+1}+\eta(\eta-1)C_s\rho^{\eta-1}\right]-\left[t_0\left(\frac{1}{2}+x_0\right)+\left(\frac{\alpha+2}{2}\right)\left(\frac{\alpha+1}{6}\right)t_3\left(\frac{1}{2}+x_3\right)\rho^{\alpha}\right.\\
&\left.\left.-\left(\frac{\beta+2}{2}\right)(\beta+1)C\rho^{\beta}-\frac{T}{2\sqrt{2}}\left(\frac{\lambda^3}{\gamma}\right)\right](2y-1)^2\left(\frac{\rho}{2}\right)+(\beta+2)(\beta+1)C\rho^{\beta}(2y-1)\left(\frac{\rho}{2}\right)\right\}d\rho\\
&-\left\{\left[t_0\left(\frac{1}{2}+x_0\right)+\left(\frac{\alpha+1}{6}\right)t_3\left(\frac{1}{2}+x_3\right)\rho^{\alpha}-(\beta+1)C\rho^{\beta}-\frac{T}{2\sqrt{2}}\left(\frac{\lambda^3}{\gamma}\right)\right](2y-1)\left(\frac{\rho}{2}\right)^2-(\beta+1)C\rho^{\beta}\left(\frac{\rho}{2}\right)^2\right\}4dy, \qquad (60)
\end{aligned}
$$

where $\tilde{b}_2=\frac{3}{8}t_0$, $\tilde{b}_3=[(\alpha+1)/16]t_3$, and $\tilde{b}_C=[(\beta+1)/4]C$. Thus we have, for a fixed $P$ and $y$,

$$
\begin{aligned}
\left(\frac{\partial\rho}{\partial T}\right)_{y,P}=&-\left\{\left[T\rho-\frac{T}{2\sqrt{2}}\left(\frac{\lambda^3}{\gamma}\right)\left(\frac{\sum_q \rho_q^2}{4}\right)\right]\right\}\frac{\rho}{T}\left\{\left[T\rho+\frac{T}{2\sqrt{2}}\left(\frac{\lambda^3}{\gamma}\right)\left(\sum_q \rho_q^2\right)\right]\right.\\
&+\left[t_0\left(1+\frac{x_0}{2}\right)\rho^2+\frac{t_3}{12}\left(1+\frac{x_3}{2}\right)(\alpha+1)(\alpha+2)\rho^{\alpha+2}-t_0\left(\frac{1}{2}+x_0\right)\left(\sum_q \rho_q^2\right)-\frac{t_3}{12}\left(\frac{1}{2}+x_3\right)(\alpha+1)(\alpha+2)\rho^{\alpha}\left(\sum_q \rho_q^2\right)\right.\\
&\left.\left.+C(\beta+1)(\beta+2)\rho^{\beta}\rho_p^2+C_s(\eta-1)\eta\rho^{\eta}\right]\right\}^{-1}\\
=&-\left\{\rho-\frac{1}{2}\frac{1}{2\sqrt{2}}\left(\frac{\lambda^3}{\gamma}\right)\left(\frac{\rho}{2}\right)^2-\frac{1}{2}\frac{1}{2\sqrt{2}}\left(\frac{\lambda^3}{\gamma}\right)(2y-1)^2\left(\frac{\rho}{2}\right)^2\right\}\\
&\times\left\{\left[T+2\tilde{b}_2\rho+(\alpha+2)\tilde{b}_3\rho^{\alpha+1}+\frac{T}{2\sqrt{2}}\left(\frac{\lambda^3}{\gamma}\right)\left(\frac{\rho}{2}\right)+(\beta+2)\tilde{b}_C\rho^{\beta+1}+\eta(\eta-1)C_s\rho^{\eta-1}\right]\right.
\end{aligned}
$$

$$-\left[t_0\left(\frac{1}{2}+x_0\right)+\left(\frac{\alpha+2}{2}\right)\left(\frac{\alpha+1}{6}\right)t_3\left(\frac{1}{2}+x_3\right)\rho^{\alpha}-\left(\frac{\beta+2}{2}\right)(\beta+1)C\rho^{\beta}-\frac{T}{2\sqrt{2}}\left(\frac{\lambda^3}{\gamma}\right)\right]$$

$$\times(2y-1)^2\left(\frac{\rho}{2}\right)+(\beta+2)(\beta+1)C\rho^{\beta}(2y-1)\left(\frac{\rho}{2}\right)\Bigg\}^{-1}. \tag{61}$$

Using this we get the specific heat capacity, from Eq. (56),

$$c_V=T\left(\frac{\partial\mathcal{S}/\rho}{\partial T}\right)_{y,V}=T\left(\frac{\partial\mathcal{S}/\rho}{\partial T}\right)_{y,\rho}=\frac{3}{2}\left[1-\frac{1}{2\sqrt{2}}\left(\frac{\lambda^3}{\gamma}\right)\frac{[1+(2y-1)^2]}{2}\left(\frac{\rho}{4}\right)\right]=\frac{3}{2}\left[\rho-\frac{1}{2\sqrt{2}}\left(\frac{\lambda^3}{\gamma}\right)\left(\frac{\sum_q\rho_q^2}{4}\right)\right]\left(\frac{1}{\rho}\right), \tag{62}$$

$$\begin{aligned}
c_P&=T\left(\frac{\partial\mathcal{S}/\rho}{\partial T}\right)_{y,P}=T\left(\frac{\partial\mathcal{S}/\rho}{\partial T}\right)_{y,\rho}+T\left(\frac{\partial\mathcal{S}/\rho}{\partial\rho}\right)_{y,T}\left(\frac{\partial\rho}{\partial T}\right)_{y,P}=c_V+\left\{-1+\frac{1}{2\sqrt{2}}\left(\frac{\lambda^3}{\gamma}\right)\frac{[1+(2y-1)^2]}{2}\left(\frac{\rho}{4}\right)\right\}\left(\frac{1}{\rho}\right)T\left(\frac{\partial\rho}{\partial T}\right)_{y,P}\\
&=c_V+\left\{T-\frac{T}{2\sqrt{2}}\left(\frac{\lambda^3}{\gamma}\right)\frac{[1+(2y-1)^2]}{2}\left(\frac{\rho}{4}\right)\right\}^2\frac{1}{T}\\
&\quad\times\Bigg\{\left[T+2\tilde{b}_2\rho+(\alpha+2)\tilde{b}_3\rho^{\alpha+1}+\frac{T}{2\sqrt{2}}\left(\frac{\lambda^3}{\gamma}\right)\left(\frac{\rho}{2}\right)+(\beta+2)\tilde{b}_C\rho^{\beta+1}+\eta(\eta-1)C_s\rho^{\eta-1}\right]\\
&\quad-\left[t_0\left(\frac{1}{2}+x_0\right)+\left(\frac{\alpha+2}{2}\right)\left(\frac{\alpha+1}{6}\right)t_3\left(\frac{1}{2}+x_3\right)\rho^{\alpha}-\left(\frac{\beta+2}{2}\right)(\beta+1)C\rho^{\beta}-\frac{T}{2\sqrt{2}}\left(\frac{\lambda^3}{\gamma}\right)\right]\\
&\quad\times(2y-1)^2\left(\frac{\rho}{2}\right)+(\beta+2)(\beta+1)C\rho^{\beta}(2y-1)\left(\frac{\rho}{2}\right)\Bigg\}^{-1}\\
&=c_V+\left\{\left[T\rho-\frac{T}{2\sqrt{2}}\left(\frac{\lambda^3}{\gamma}\right)\left(\frac{\sum_q\rho_q^2}{4}\right)\right]\right\}^2\left(\frac{1}{\rho}\right)\left(\frac{1}{T}\right)\left\{\left[T\rho+\frac{T}{2\sqrt{2}}\left(\frac{\lambda^3}{\gamma}\right)\left(\sum_q\rho_q^2\right)\right]\right.\\
&\quad+\left[t_0\left(1+\frac{x_0}{2}\right)\rho^2-t_0\left(\frac{1}{2}+x_0\right)\left(\sum_q\rho_q^2\right)+\frac{t_3}{12}\left(1+\frac{x_3}{2}\right)(\alpha+1)(\alpha+2)\rho^{\alpha+2}-\frac{t_3}{12}\left(\frac{1}{2}+x_3\right)(\alpha+1)(\alpha+2)\rho^{\alpha}\left(\sum_q\rho_q^2\right)\right.\\
&\quad\left.\left.+C(\beta+1)(\beta+2)\rho^{\beta}\rho_p^2+C_s(\eta-1)\eta\rho^{\eta}\right]\right\}^{-1}.
\end{aligned} \tag{63}$$

The difference of $c_P$ and $c_V$ is proportional to $(\partial\rho/\partial T)$. This shows that even though the specific heat with fixed volume $c_V$ has no divergence, there may be a divergence in the specific heat with fixed pressure $c_P$ at some $T$ showing a first order phase transition if $(\partial\rho/\partial T)_{y,P}=\infty$, i.e., $(\partial T/\partial\rho)_{y,P}=0$. This happens when $(\partial y/\partial\rho)_{T,P}=0$ according to Eq. (60). However, if this happens in the coexistence region, then this discontinuity does not contribute to the phase transition and the phase transition will be second order depending on other conditions.

### III. PHASE TRANSITION OF A FINITE NUCLEUS WITH A COULOMB INTERACTION

In this section we present results of our calculations of the phase transition of a finite asymmetric nucleus. The results are based on the equations developed in the previous section which arise from a Skyrme interaction and include the effects of Coulomb and surface terms besides the symmetry term. Here we use the Skyrme interaction of PRC45 in Table I with $\beta=0$, $\eta=2/3$, the surface energy $4\pi r_0^2\sigma=20.0$ MeV, and $R=6$ fm. We restricted our analysis only to the Skyrme interaction with $x_3=-1/2$ here. With this choice, there is no crossing of $P(\rho)$ curves between different values of $y$ at fixed $T$ which is a behavior similar to that in Ref. [7]. With $x_3\neq-1/2$, the nonlinear dependence of the symmetry energy on $\rho$ causes a crossing of the $P(\rho)$ curves between different values of $y$ at some density and thus the minimum pressure occurs at different $y$ values for different density $\rho$ [see Eq. (60)] for a given $T$. This makes the analysis for the phase diagram more complicated. In this paper, using $x_3=-1/2$, we concentrate on the effect of the Coulomb interaction by

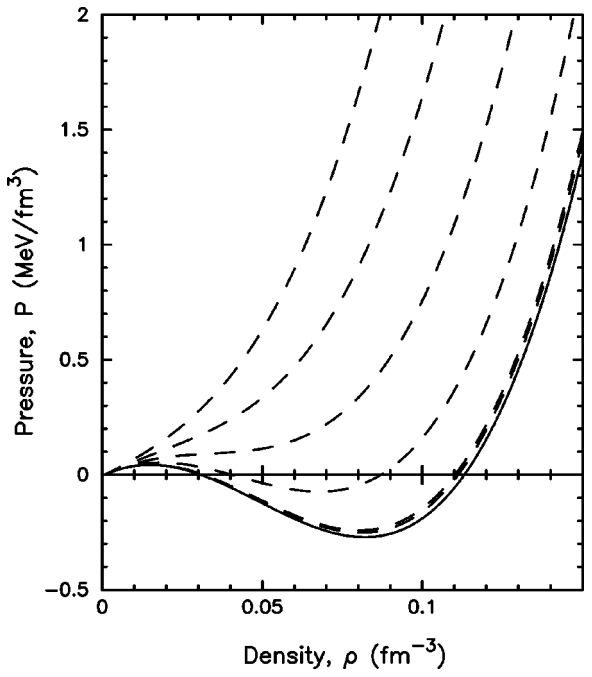


FIG. 1. Pressure $P(\rho)$ versus $\rho$ at $T=10$ MeV for various $y$. The dashed curves from top to bottom have $y=0$, 0.1, 0.2, 0.3, 0.4, and 0.5 while the solid curve is for $y=0.4552$.

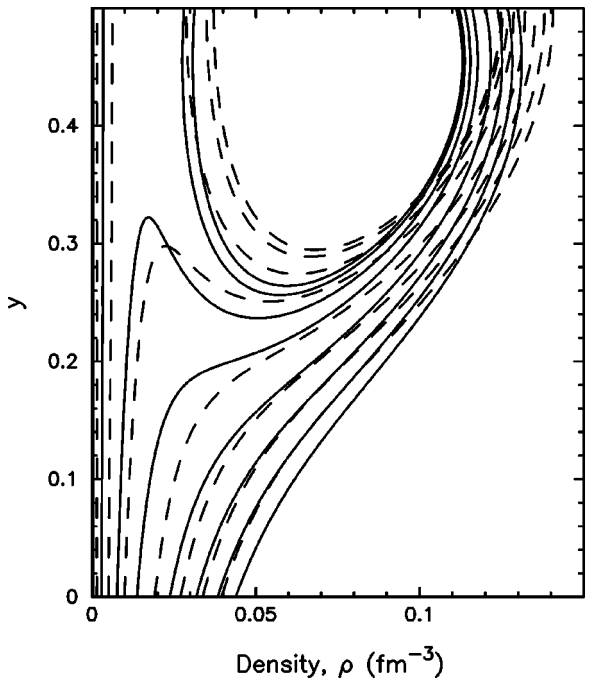


FIG. 2. Proton fraction $y(\rho)$ for $P=0$, 0.015, 0.05, 0.1, 0.2, 0.3, 0.4, and 0.5, from top to bottom, at $T=10$ MeV. The solid curves have Coulomb and surface tension contributions and the dashed curves are without these interactions.

comparing with the results of Ref. [7].

Figure 1 shows the pressure $P(\rho)$ for various $y$ values at $T=10$ MeV. The values of $y$ used range from $y=0$ (neutron matter) to $y=0.5$ (symmetric systems). Some important features of this figure are the following. Above a certain $y=y_c$ the curves have a characteristic S shape. This is the well-known behavior of a van der Waals–like equation of state with long range attraction and short range repulsion. For one-component systems this behavior leads to a Maxwell construction and the end points of the Maxwell line define the liquid-gas boundary. The region between the maxima and minima of the $P(\rho)$ curve has negative compressibility and is the spinodal instability region. For two-component systems, because of the extra degree of freedom associated with varying proton fraction in a system with two phases, the phase diagram has a higher dimensionality. One effect of this higher dimensionality is to change a first-order transition into a second-order transition as noted in Refs. [7,8]. Another effect is that the phase diagram is now a surface in pressure $P$, temperature $T$, and proton fraction $y$ or nucleon density $\rho$. At a particular $y=y_c(T)$, the CP for given temperature $T$, the S shape disappears. Below this $y_c$, there is no longer a liquid-gas boundary for this $T$. The existence of a critical point $y_c$ is similarly seen in Ref. [7]. The Coulomb interaction has new effects also. For $T=10$ MeV, the lowest pressure occurs not at $y=1/2$ but at $y=0.4552$ for $R=6$ fm due to the Coulomb repulsion independent of the surface tension [see Eqs. (54) or (60)]. This $y$ value, for $x_3=-1/2$, is also independent of $\rho$. For $R=10$ fm, the lowest pressure occurs at $y=0.3927$ due to a stronger Coulomb effect. According to Eqs. (54) or (60), the $y$ value having minimum pressure approaches $y=0.5$ as $T$ increases.

Let us next turn to Fig. 2 which is based on the following property. For fixed $P$ and $T$, $y$ and $\rho$ are not independent. Since Eq. (54) is a second order equation for $y$, $y$ can in general have two values for a given density $\rho$. Equation (58) expresses the dependence of $y$ on $\rho$ for a given $P$ and $T$. This equation is an important result in our method of analysis of the liquid-gas phase transition in asymmetric systems. In particular, Eq. (58) allows us to find the energy and entropy as a function of $P$, $y$, and $T$ using Eqs. (55) and (56), respectively. Figure 2 shows the proton fraction $y(\rho)$ for various $P$ values at $T=10$ MeV. Here only the $0\leqslant y\leqslant 0.5$ region is shown. These curves show a backbending feature for large $y$ with $\partial\rho/\partial y=0$ at $y=0.4552<1/2$ for the $R$ parameter of the Coulomb interaction taken as 6 fm. At this $y$ value of backbending $[(\partial\rho/\partial y)=0]$, the pressure is minimum $[(\partial P/\partial y)=0]$ too as can be seen from Eqs. (58) and (60). For $R=10$ fm, the backbending occurs at $y=0.3927$. Without a Coulomb interaction, there is no backbending in the $0\leqslant y\leqslant 0.5$ region and $\partial\rho/\partial y=0$ at $y=1/2$. The discontinuity of $y(\rho)$ at low density for small pressure is expected from the low density region of Fig. 1.

Figure 3 shows a plot of the chemical potential for protons $\mu_p(y)$ and neutrons $\mu_n(y)$ as a function of the proton fraction $y$ for several values of $P$ and at $T=10$ MeV. From this figure we can find the binodal points by using Eq. (30). In particular the equality of the chemical potentials at the same $P$ and $T$ determines two values of $y$ at the phase boundaries, one for the liquid phase and one for the gas phase. Specifically $\mu_n(P,y_1,T)=\mu_n(P,y_2,T)$ and $\mu_p(P,y_1,T)=\mu_p(P,y_2,T)$. A geometric construction of this equality would be a rectangular box in Fig. 3 as shown in Fig. 6 of Ref. [7]. The vertical sides of this rectangle are the two val-

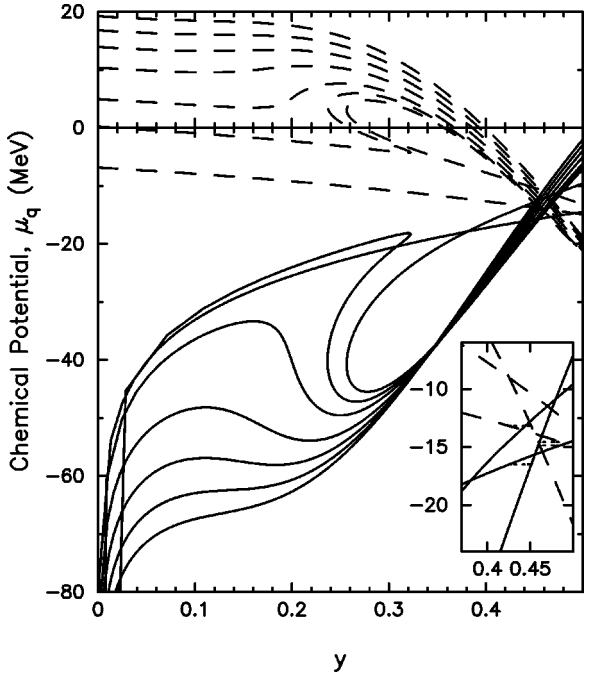


FIG. 3. Chemical potential $\mu_p(y)$ and $\mu_n(y)$ for $P=0.015$, 0.05, 0.1, 0.2, 0.3, 0.4, and 0.5, from top to bottom curve for protons (solid curve) and bottom to top for neutrons (dashed curve) at $T=10$ MeV. The chemical potential increases as the pressure increases at $y=1/2$. For smaller $y$, $\mu_n$ increases and $\mu_p$ decreases as $P$ increases except $\mu_p$ for $P=0.015$ and 0.05. The small box at the right-bottom corner is the expanded curve for $P=0.015$ MeV/fm$^3$ with two pairs of binodal points indicated by dotted lines.

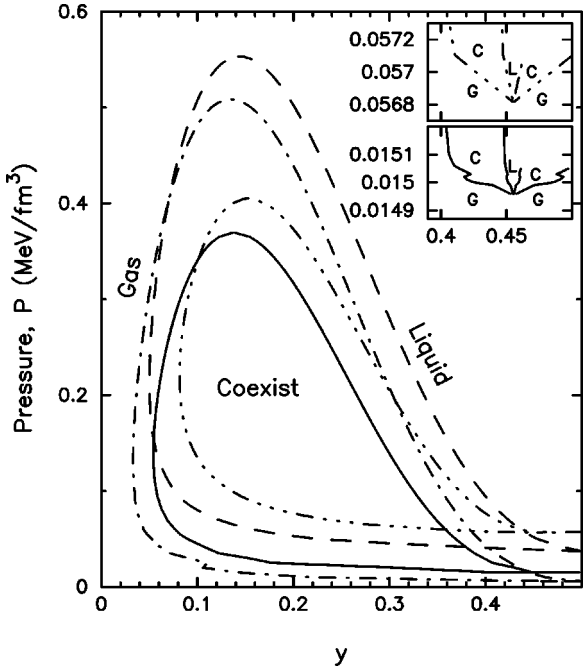


FIG. 4. Binodal curve at $T=10$ MeV. The solid curve is for the case with Coulomb and surface effects, the dash-dotted curve is for the case with surface effects, the dash-dot-dot-dotted curve is for the case with Coulomb interactions, and the dashed curve is for the case without Coulomb and surface effects. Small boxes at the upper right corner are the expansion of the main figure. In the small boxes, the region of liquid, gas, and coexistence are indicated by L, G, and C, respectively.

ues of $y$, $y_1$, and $y_2$, and the horizontal sides are the two chemical potentials $\mu_n$ and $\mu_p$. For each $P$ and $T$ with $T \leqslant T_c$ with $T_c$ the critical temperature, a pair of $y$'s can be found and are the binodal points for that $P$ and $T$. Fixing just $T$ and varying $P$ generates a binodal loop of $P$ versus $y$ as shown in Fig. 4. While the overall qualitative behavior shown in this figure is similar to that of Ref. [7], the quantitative results are different because of the Coulomb and surface terms that our approach contains. Moreover, an interesting new feature arises from the Coulomb term since $\mu_p > \mu_n$ at $y=1/2$ instead of $\mu_p=\mu_n$. Specifically, the Coulomb interaction leads to the crossing of the neutron and proton chemical potentials in the range of $y>0.4$ for the Skyrme parameter used here. The Coulomb interaction also leads to the crossing of the small density portion and the high density portion of the proton chemical potential $\mu_p$ at fixed $P$ and $T$ while the crossing of the small density and the high density portions of the neutron chemical potential $\mu_n$ at fixed $P$ and $T$ was seen in Ref. [7] too. These new crossings due to the Coulomb effect bring in a new pair of binodal points for low pressure. An expanded view of these crossings is shown in the box at the right-bottom corner of Fig. 3 for a pressure $P=0.015$ MeV/fm$^3$. This small box has two pairs of binodal points indicated by the horizontal dotted lines which correspond to the horizontal sides of the rectangle mentioned above. This small box shows one pair at a slightly lower $y$ than $y=0.4552$ and another pair slightly above $y=0.4552$. These two pairs of binodal points also show up in the phase diagram. Their effect is shown in the box at the right-upper corner of Fig. 4 which will now be discussed.

Figure 4 shows the coexistence binodal loop in the $y$-$P$ plane at $T=10$ MeV. The figure shows that the major effect of the surface tension is a lowering of the pressure for the coexistence curve (compare the dash-dotted curve vs dashed curve and the solid curve vs dash-dot-dot-dotted curve). The inclusion of surface tension may allow for a zero-pressure isobaric phase transition and may simulate the situation of an equilibrated state of multifragmentation having zero internal pressure for stable finite nuclei with nonzero gas pressure as discussed in Ref. [9]. The effect of the Coulomb interaction makes the coexistence region smaller. However, a more important effect of the Coulomb interaction is the appearance of another pair of binodal points in the low pressure region (see the expanded figure in the box at the right-upper corner). Two points of smaller $y$ values have the same chemical potential and two points of larger $y$ values have the same chemical potential. However, they are different from each other, with the larger $y$ pair having larger $\mu_p$ and smaller $\mu_n$ than the corresponding values of the other pair with smaller $y$ (see Table II). Here the points with largest and smallest $y$ value are in gas phase and the points between the other two $y$ values are in the liquid phase [see Table II; Eq. (58) shows that there are two values of $y$ for a given $\rho$ at fixed $P$ and $T$]. The binodal pair with higher $y$ values allows the mixture of gas with highest $y$ and liquid with the next high $y$ and is a reversed situation from the other binodal pairs and the

TABLE II. Coexistence points.

| $P$ (MeV/fm$^3$) | $\rho$ (fm$^3$) | $y$ | $\mu_p$ (MeV) | $\mu_n$ (MeV) |
|---|---|---|---|---|
| 0.01496 | 0.0034324 | 0.4526870 | −15.73360 | −13.80920 |
| | 0.1138296 | 0.4548638 | −15.73360 | −13.80920 |
| | 0.1138296 | 0.4555570 | −15.59369 | −13.92612 |
| | 0.0034324 | 0.4577830 | −15.59369 | −13.92612 |
| 0.01498 | 0.0034352 | 0.4441228 | −15.97430 | −13.61531 |
| | 0.1138098 | 0.4536912 | −15.97430 | −13.61531 |
| | 0.1138096 | 0.4567391 | −15.35914 | −14.12939 |
| | 0.0034352 | 0.4665239 | −15.35914 | −14.12939 |
| 0.01500 | 0.0034373 | 0.4253351 | −16.50124 | −13.19126 |
| | 0.1137651 | 0.4511254 | −16.50124 | −13.19126 |
| | 0.1137652 | 0.4592869 | −14.85386 | −14.56769 |
| | 0.0034372 | 0.4853333 | −14.85386 | −14.56769 |
| 0.01503 | 0.0034421 | 0.4226954 | −16.57709 | −13.12985 |
| | 0.1137598 | 0.4507550 | −16.57709 | −13.12985 |
| | 0.1137592 | 0.4596993 | −14.77187 | −14.63844 |
| | 0.0034420 | 0.4883935 | −14.77187 | −14.63844 |
| 0.01505 | 0.0034449 | 0.4141177 | −16.81862 | −12.93537 |
| | 0.1137397 | 0.4495787 | −16.81862 | −12.93537 |
| | 0.1137389 | 0.4608853 | −14.53660 | −14.84241 |
| | 0.0034448 | 0.4971483 | −14.53660 | −14.84241 |
| 0.01506 | 0.0034463 | 0.4102457 | −16.92777 | −12.84748 |
| | 0.1137306 | 0.4490471 | −16.92777 | −12.84748 |

result of Ref. [7]. This allows for a phase separation into a liquid phase with fewer protons (lower $y$ value) and a gas phase with more protons (higher $y$ value) which is more realistic in heavy ion collisions. For the Skyrme parameter we used here with $x_3=-1/2$, the two pairs of binodal points meet at one point in $y$, having a minimum $P$ for a given $T$ as shown in the small box in this figure. At this point, both the liquid and gas phases have the same proton concentration (EC) $y=y_E$ with different density $\rho$. If the initial overall concentration $y$ is greater than the equal concentration $y_E$, then the system ends up with more proton concentration in gas and less proton concentration in liquid phase. If the initial $y$ were smaller than $y_E$, then the final system has more proton concentration in liquid phase and less proton concentration in gas phase. The equal concentration point $y_E$ is independent of the surface energy and nucleon density $\rho$ and approaches $y=0.5$ as $T$ increases as can be seen from Eqs. (54) or (60). The value of equal concentration $y_E$ decreases as the Coulomb interaction increases; here $y_E=0.4552$ for $R=6$ fm and it would be changed to $y_E=0.3927$ for $R=10$ fm. Without the Coulomb interaction the $y_E$ becomes $y_E=0.5$, the proton ratio for a symmetric system as seen in Ref. [7]. If $x_3\neq-1/2$, as a result of the nonlinear $\rho$ dependence of the symmetry energy, the pressure $P$ becomes minimum $[(\partial P/\partial y)_T=0]$ at a different $y$ value for the liquid and gas phases. For this case, unless the minimum pressure of liquid is lower than the minimum pressure of gas, there would be no point of EC. This should be studied further.

The results of Eqs. (54) or (58) can be used to obtain a connection between $T$ and $\rho$ for each $P$ and $y$. Figure 5 shows $T(\rho)$ for various $P$ values at $y=0.3$ and 0.5. This figure shows that at a low pressure there are two points with $(\partial T/\partial\rho)_{y,P}=0$, i.e., $(\partial\rho/\partial T)_{y,P}=\infty$, which may cause a discontinuity in $c_P$ according to Eq. (63). According to Eq. (60), $(\partial T/\partial\rho)_{y,P}=0$ when $(\partial P/\partial\rho)_{y,T}=0$, i.e., at the spin-

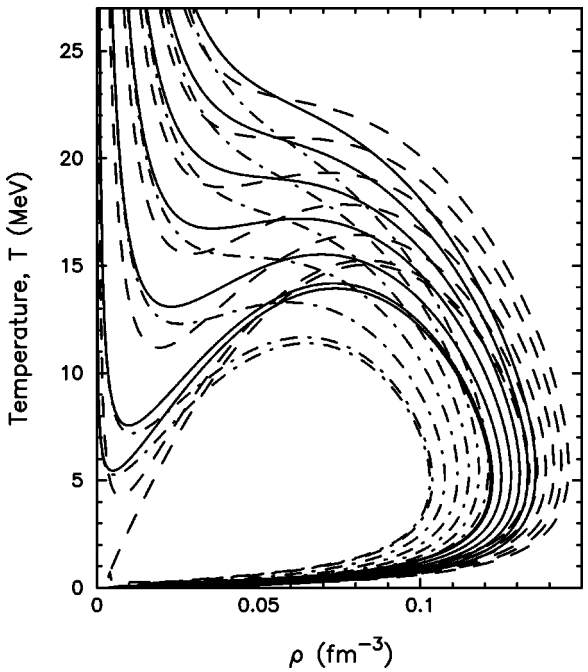


FIG. 5. Temperature $T(\rho)$ for $P=0.0$, 0.015, 0.1, 0.2, 0.3, 0.4, and 0.5, from bottom to top, at $y=0.3$ (dash-dotted curve) and 0.5 (solid curve). Dashed curves are for the case without Coulomb and surface effects.

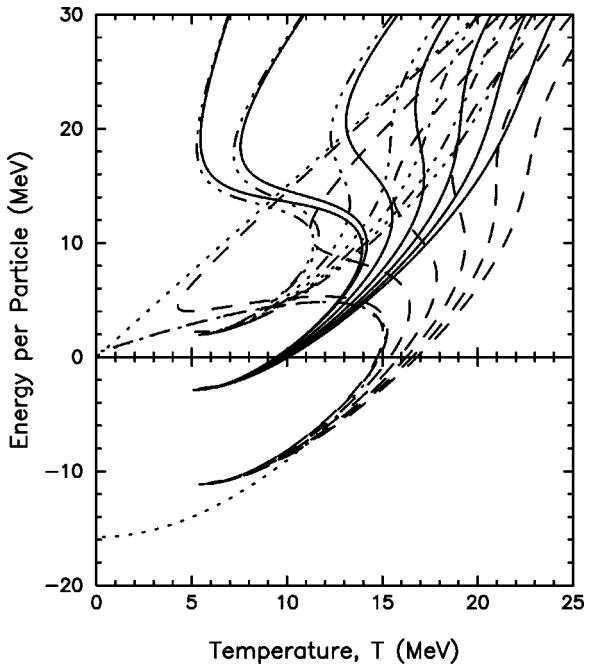


FIG. 6. Energy per particle $\mathcal{E}(T)/\rho$ for $P=0.0$, 0.015, 0.1 0.2, 0.3, 0.4, and 0.5, from top to bottom, at $y=0.3$ (dash-dot-dot-dotted curve) and 0.5 (solid curve). Dashed curves are for $y=0.5$ without Coulomb and surface effects and the dotted line is for the exact result at $P=0$ from Ref. [16]. This shows that the Fermi gas approximation we have used is not valid for $T$ lower than about 5 MeV with high density, but very accurate for higher temperature (the dashed curve for $P=0.0$ coincides with the dotted curve for $\mathcal{E}/\rho \geqslant 8$ MeV).

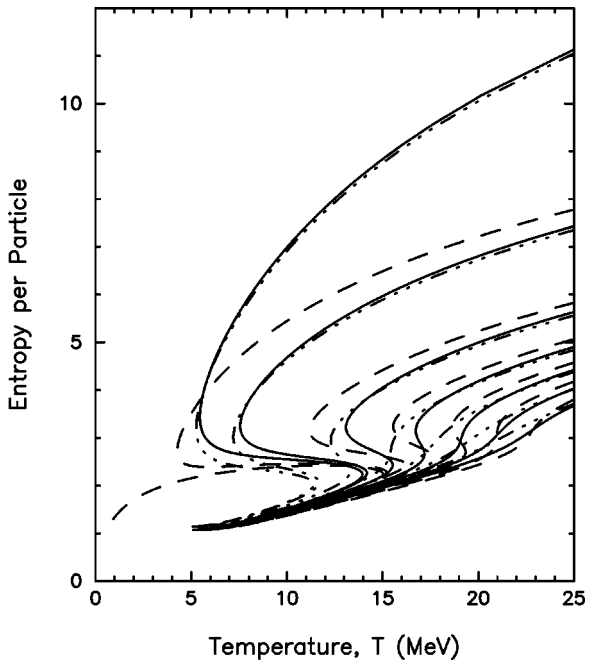


FIG. 7. Same as Fig. 6 but for entropy per particle $\mathcal{S}(T)/\rho$.

odal points. Equation (60) also shows that $[\partial(\mathcal{E}/\rho)/\partial T]_{y,P} = \infty$ and $[\partial(\mathcal{S}/\rho)/\partial T]_{y,P}=\infty$ at the spinodal points having $(\partial P/\partial\rho)_{y,T}=0$. Thus by investigating the behavior of energy and entropy as the temperature $T$ changes, we can study the behavior of heat capacity $c_P$ or the order of the phase transition.

Figures 6 and 7 shows $(\mathcal{E}/\rho)_{y,P}$ and $(\mathcal{S}/\rho)_{y,P}$ as a function of $T$ for various $P$ values at $y=0.3$ and 0.5. The overall $T$ dependence is qualitatively same as in Ref. [7]. Comparing with the exact result of Ref. [16] (dotted curve in Fig. 6), we can see that the high $T$ nondegenerate Fermi gas approximation used here is good for the region which corresponds to $\mathcal{E}/\rho > 8$ MeV for the case without Coulomb and surface effects. For lower energy and lower $T$, we need to use a degenerate Fermi gas limit which has more complicate $y$ dependence than the nondegenerate Fermi gas limit [see Eqs. (49)–(52)] and the simple relation (58) is no longer applicable. The points with diverging slope of $\mathcal{E}/\rho$ and $\mathcal{S}/\rho$ in variations of $T$ are related to the zero-slope points in Fig. 5. If the charge concentration $y$ were kept constant in all phases during adiabatic heating of the system at fixed pressure $P$, then the system follows one curve in Figs. 6 and 7 with the corresponding $y$ and $P$ similar to a one-component system. If we follow a curve in Fig. 6 as the energy increases, then the temperature goes up until it first reaches the spinodal point at higher $T$ and lower energy before reaching the spinodal point at lower $T$ and higher energy. Since both spinodal points are inside of the coexistence region, the diverging slope of energy and entropy at spinodal points and $(\partial T/\partial\rho)_{y,P}=0$ do not contribute to the phase transition. However, because of the backbending of the curves in Figs. 6 and 7 for low pressure, the energy jumps at the binodal points and it can cause a first-order phase transition if all the phases have the same $y$ which is similar to a one-component system. But as discussed in detail in Ref. [7], in the actual phase transition of a heavy ion collision with two components, the proton fraction $y$ in each phase can be different while still conserving the overall fraction. Because of the mixing of phases with different $y$ values, the transition becomes a second-order phase transition [7]. Since the $T$ dependence of the energy and entropy for fixed $y$ and $P$ (Figs. 6 and 7) is qualitatively same as in Ref. [7], the characteristic of phase transition here will be the same as the result of Ref. [7].

## IV. SUMMARY AND CONCLUSION

In this paper we studied the liquid-gas phase transition in a two-component hadronic system made of protons and neutrons. The analysis of the thermodynamic properties of asymmetric nuclei with arbitrary proton-neutron ratios is important in several areas such as in astrophysical situations where neutron stars are of interest and in radioactive beam studies. Such studies are considerably more complicated than a one-component system or a symmetric system of protons and neutrons without Coulomb interactions. A novel aspect of asymmetric systems is the possibility of having different proton-neutron ratios in each of the phases, while still conserving the overall initial proton fraction. This feature arises from the symmetry energy which prefers equal numbers of protons and neutrons in denser regions, but its effect is moderated by the Coulomb force. Such features are well known from the $N$-$Z$ behavior of stable nuclei where for light nuclei

$N=Z$ but for heavy nuclei $N>Z$. Because of the extra degree of freedom associated with varying proton fraction in a system with two phases, the phase diagram has a higher dimensionality. One effect of this higher dimensionality is to change a first-order transition [18] into a second-order transition as noted in Refs. [7,8]. Another effect is that the phase diagram is now a surface in pressure $P$, temperature $T$, and proton fraction $y$ or nucleon density $\rho$ [7]. For a given $A=N+Z$ stability is determined by both Coulomb and surface effects in addition to the symmetry energy. This paper is a study of the additional role of Coulomb and surface effects on the thermodynamic properties of heated nuclei.

Our investigation of the phase diagram was carried out using a Skyrme interaction and the approach was based on a mean field theory. In Sec. II, the main equations were given for multicomponent systems where the use of the Skyrme interaction for a two-component nuclear system was shown to simplify expressions so that the results are analytic functions of $P$, $T$, and $y$: Eqs. (53)–(56) with Eq. (58). These expressions include the pressure and both neutron and proton chemical potentials $\mu_n$ and $\mu_p$. Phase equilibrium requires equality of $\mu_n$ between the two phases and similarly $\mu_p$ at the same $P$ and $T$. At fixed $T$ and $P$, $\rho$ and $y$ are not independent [Eq. (58) and Fig. 2] and we use this property in our model to further simplify its analysis. This connection also allowed us to find the energy and entropy as a function of $P$, $y$, and $T$ (Figs. 6 and 7).

Our mean field approach using a Skyrme interaction is an extension of a previous study initially begun in Ref. [1] for two components and the analysis is similar in some ways to that developed in Ref. [7]. However, in this paper we included surface and Coulomb effects so our results differ quantitatively from those in Ref. [7]. The Coulomb interaction and surface tension are incorporated into the description by treating the system as a uniformly charged sphere with a fixed value of $R$. While somewhat simplified we feel that results obtained from it may be a useful instructive example of the qualitative effects that the Coulomb interaction and surface tension have on the binodal surface. Some features of the results are similar qualitatively with the results of Ref. [7]. For example, the temperature dependence of the energy and entropy (Figs. 6 and 7) is qualitatively the same as the result of Ref. [7] which indicates the phase transition is second order. However, including Coulomb and surface effects introduces some features also not present in Ref. [7] which are summarized below. Since the $T$ dependence of our results is similar with the results of Ref. [7], we considered here only a high temperature nondegenerate Fermi gas limit which has much simpler density dependence of the kinetic energy and pressure than a low temperature limit [see Eqs. (49)–(52) and Eq. (54)].

The importance of surface energies in the liquid-gas phase transition was shown in Refs. [3,4] using an approach based on a statistical model of multifragmentation. In the statistical model of multifragmentation, because nuclear matter can be broken into a large number of small pieces, the surface energy plays a very dominant role [18,19]. Here, in a mean field theory, the surface energy plays a lesser role since we do not allow for the possibility of multifragmentation. Rather, the system is treated as uniform but with varying density. One effect of the surface tension in our study is to bring the coexistence binodal surface to lower pressure which could allow for an isobaric transition at zero pressure (see Fig. 4). It may simulate a situation of an equilibrated state of multifragmentation where stable finite nuclei have zero internal pressure but nonzero gas pressure [9]. The surface effect becomes larger as the size $R$ becomes smaller and we can bring binodal surface to cross $P=0$ plane.

Inclusion of the Coulomb interaction brings a new feature in the mean field approach. Figure 4 showed the shrinking of the binodal loop from the inclusion of the Coulomb term. The effect of the Coulomb force in reducing the dynamical instability region is also seen in RPA-type calculations [10,12]. Figure 4 also contains the effects of the surface term. Moreover, the contribution of each term, Coulomb only, surface only, and both Coulomb and surface are compared with a situation without Coulomb and surface terms. This comparison enabled us to isolate the importance and role of these various contributions. Figure 3 showed the effect of the Coulomb force on the proton chemical potential and it leads to a crossing of the proton chemical potentials and neutron chemical potentials for different values of $P$ and $y$ near $y=0.5$.

The Coulomb interaction also brings the line of equal concentration of protons (LEC) on the binodal surface to a smaller $y=y_E$ value than $y=0.5$ for the symmetric system. It also causes another pair of binodal points with $y>y_E$ at low pressure with a reversed proton fraction in the liquid-gas phase, i.e., with fewer protons in the liquid phase and more protons in the gas phase. At the proton fraction $y_E$ two pairs of binodal points meet together and the pressure becomes smallest on the binodal curve as can be seen in the box in Fig. 4. This value of $y_E$ can be made smaller by using a stronger Coulomb interaction with larger $R$. For the case of $x_3=-1/2$, the point of equal concentration $y_E$ is directly related to the backbending point of $y(\rho)$ shown in Fig. 2 and also to the point with minimum pressure on the binodal loop in Fig. 4 and on the $P(\rho)_{y,T}$ curve in Fig. 1. If the initial overall $y$ is greater than $y_E$, then the phase transition ends up with a larger proton fraction in the gas and a smaller $y$ in the liquid phase. On the other hand, for the initial $y<y_E$, the system ends up with a larger $y$ in liquid and smaller $y$ in gas phase. Equation (58) shows that the value of $y_E$ is independent of the density $\rho$ for $x_3=-1/2$ and approaches $y_E=0.5$ as $T$ increases. The new pair of binodal points with $y>y_E$ disappears as $y_E$ reaches 0.5, the proton ratio for a symmetric system.

In this paper we used a fixed value of $R$ to determine the strength of Coulomb interaction and surface tension. Here, if we increase the strength of Coulomb effect by increasing the value of $R$, then the surface tension decreases. If we allow for variations of $R$ with $\rho$ or $T$ and allow different values for the Coulomb and surface energies, then this simple model may be used to study multifragmentation with various sizes of clusters. We also restricted the symmetry energy per particle to have only a linear dependence on the nucleon density. Allowing a higher order $\rho$ dependence of the symmetry energy through $x_3\neq-1/2$, the EC point might be destroyed.

The nonlinear $\rho$ dependence of the symmetry energy causes a crossing between $P(\rho)$ curves for different values of $y$ at a given $T$. Because of this crossing, the liquid phase portion and the gas phase portion of the binodal curve have minimum pressure at different $y$ values and possibly do not meet in the range of $0 \leqslant y \leqslant 0.5$. These features should be investigated further.

**ACKNOWLEDGMENTS**

This research was supported by the U.S. DOE, Grant No. DE-FG02-96ER-40987. S.J.L. gratefully acknowledges support for a sabbatical leave from Kyung Hee University and a sabbatical year at Rutgers University.

[1] H.R. Jaqaman, A.Z. Mekjian, and L. Zamick, Phys. Rev. C **29**, 2067 (1984).
[2] J.E. Finn *et al.*, Phys. Rev. Lett. **49**, 1321 (1982).
[3] A.S. Hirsch *et al.*, Phys. Rev. C **29**, 508 (1984).
[4] L.P. Csernai and J.I. Kapusta, Phys. Rep. **131**, 223 (1986).
[5] W. Lynch, Annu. Rev. Nucl. Sci. **37**, 493 (1987).
[6] S. Das Gupta, A.Z.Mekjian, and B. Tsang, in *Advances in Nuclear Physics*, Vol. 26, edited by J. Negele and E. Vogt (Plenum, New York, 2000).
[7] H. Müller and B.D. Serot, Phys. Rev. C **52**, 2072 (1995).
[8] N.K. Glendenning, Phys. Rev. D **46**, 1274 (1992).
[9] S.J. Lee and A.Z. Mekjian, Phys. Rev. C **56**, 2621 (1997).
[10] G. Fabbri and F. Matera, Phys. Rev. C **58**, 1345 (1998).
[11] V. Baran, M. Colonna, M. Di Toro, and A.B. Larionov, Nucl. Phys. **A632**, 287 (1998).
[12] B. Jacquot, M. Colonna, S. Ayik, and Ph. Chomaz, Nucl. Phys. **A617**, 356 (1997).
[13] G.F. Bertsch and S. Das Gupta, Phys. Rep. **160**, 189 (1988).
[14] P. Ring and P. Schuck, *The Nuclear Many-Body Problem* (Springer-Verlag, New York, 1980); S.J. Lee, Phys. Rev. C **42**, 610 (1990).
[15] C. Gale, G.M. Welke, M. Prakash, S.J. Lee, and S. Das Gupta, Phys. Rev. C **41**, 1545 (1990).
[16] S.J. Lee and A.Z. Mekjian, Phys. Rev. C **45**, 1284 (1992).
[17] K. Huang, *Statistical Mechanics* (Wiley, New York, 1987).
[18] S. Das Gupta and A.Z. Mekjian, Phys. Rev. C **57**, 1361 (1998).
[19] P. Bhattacharyya, S. Das Gupta, and A.Z. Mekjian, Phys. Rev. C **60**, 064625 (1999).